APPLIED PHYSICS

Observation of inverse Edelstein effect in Rashba-split 2DEG between $SrTiO_3$ and $LaAlO_3$ at room temperature

Qi Song,[1,2]* Hongrui Zhang,[3]* Tang Su,[1,2] Wei Yuan,[1,2] Yangyang Chen,[1,2] Wenyu Xing,[1,2] Jing Shi,[4†] Jirong Sun,[3†] Wei Han[1,2†]

The Rashba physics has been intensively studied in the field of spin orbitronics for the purpose of searching novel physical properties and the ferromagnetic (FM) magnetization switching for technological applications. We report our observation of the inverse Edelstein effect up to room temperature in the Rashba-split two-dimensional electron gas (2DEG) between two insulating oxides, $SrTiO_3$ and $LaAlO_3$, with the $LaAlO_3$ layer thickness from 3 to 40 unit cells (UC). We further demonstrate that the spin voltage could be markedly manipulated by electric field effect for the 2DEG between $SrTiO_3$ and 3-UC $LaAlO_3$. These results demonstrate that the Rashba-split 2DEG at the complex oxide interface can be used for efficient charge-and-spin conversion at room temperature for the generation and detection of spin current.

INTRODUCTION

In 1990, Edelstein predicted that spin current could be induced by charge current flowing in inversion asymmetric two-dimensional electron gases (2DEGs), which is often referred to as the Edelstein effect (EE) (*1*). The magnitude of EE highly depends on the Rashba spin-orbit coupling, which provides a locking between the momentum and spin polarization directions (*2*). The generated spin current density could be described in the following form

$$J_S \propto \alpha_R(\hbar/e)(\vec{z} \times \vec{j}_C) \quad (1)$$

where α_R is the Rashba parameter, $\vec{z}$ is the interfacial electric field direction perpendicular to the 2DEG, and $\vec{j}_C$ is the charge current. The opposite of EE is often called inverse Edelstein effect (IEE), which means that spin accumulation in inversion asymmetric 2DEG could generate an in-plane electric field perpendicular to the spin polarization direction (*3*). Because of the potential highly efficient spin-and-charge conversion, both the EE and IEE have attracted a great deal of interest for spintronics, and various experiments have been performed on the Rashba interfaces between two metallic films (*4*–*7*), two-dimensional materials (*8*–*12*), and the topological surface states (*13*–*18*).

Here, we report our observation of the IEE in the Rashba-split 2DEG between two insulating oxides, $SrTiO_3$ and $LaAlO_3$, up to room temperature. The spin current in the 2DEG is generated by spin pumping from a ferromagnetic $Ni_{80}Fe_{20}$ (Py) electrode through a $LaAlO_3$ layer with a thickness of up to 40 unit cells (UC). The IEE is probed by measuring the electric voltage that is created by the spin-to-charge conversion of the injected spin current due to the Rashba spin-orbit coupling of the 2DEG. Furthermore, we demonstrate that the spin voltage in the Rashba-split 2DEG between $SrTiO_3$ and 3-UC $LaAlO_3$ could be switched on and off using a perpendicular electric field. These results show that the complex oxide interface, which has been proven to show many interesting physical properties (*19*–*23*), can be used for efficient charge-and-spin conversion (which is gate-controllable) for the spin current generation, the spin detection, and the manipulation of the magnetization.

RESULTS

The Rashba-split 2DEG is formed between the (001)-oriented $SrTiO_3$ and $LaAlO_3$, as shown in Fig. 1A (*24*, *25*). The $LaAlO_3$ layers from 3 to 40 UC are grown on $SrTiO_3$ substrates via pulsed laser deposition (see Materials and Methods for details), and the $LaAlO_3$ thickness is monitored by in situ reflective high-energy electron diffraction (RHEED) oscillations, as shown in Fig. 1B. Figure 1C illustrates the expected qualitative energy diagram of the Rashba-split 2DEG thus obtained. At the Fermi level (E_F), the spin textures of the outer and inner circles are opposite to each other. Whether the spin texture is clockwise or counterclockwise depends on the sign of α_R and the definition of the normal direction (*26*). The α_R for the 2DEG at the interface between $SrTiO_3$ and $LaAlO_3$ is gate-tunable and is up to 5×10^{-12} eVm, based on a previous weak antilocalization measurement at 1.5 K (*27*).

The spin injection experiment is performed via spin pumping, which is a widely used technique to probe the spin-to-charge conversion in nonmagnetic materials (*4*, *10*, *17*, *28*–*32*). When the ferromagnetic resonance (FMR) condition for Py is fulfilled under the radio frequency (RF) microwave field, a spin current is injected into the Rashba-split 2DEG owing to the angular momentum conservation rule. The IEE of the spin current gives rise to an electric field that is in-plane and perpendicular to the spin polarization direction, as shown in Fig. 1D. This electric field could be detected by measuring the voltage on the two ends of the 2DEG at the interface of $SrTiO_3/LaAlO_3$ (see Materials and Methods for details).

Figure 2A shows a typical FMR spectrum of Py on the $SrTiO_3$/6-UC $LaAlO_3$ sample under the RF frequency of 6 GHz (see Materials and Methods for details), where S_{21} is the forward amplitude of the complex transmission coefficients. The magnetization dynamics of Py follows the Landau-Lifshitz-Gilbert equation (*33*, *34*)

$$\frac{d\vec{M}}{dt} = -\gamma\vec{M} \times \vec{H}_{eff} + \frac{\alpha}{M_S}\vec{M} \times \frac{d\vec{M}}{dt} \quad (2)$$

[1]International Center for Quantum Materials, School of Physics, Peking University, Beijing 100871, China. [2]Collaborative Innovation Center of Quantum Matter, Beijing 100871, China. [3]Beijing National Laboratory for Condensed Matter Physics and the Institute of Physics, Chinese Academy of Sciences, Beijing 100190, China. [4]Department of Physics and Astronomy, University of California, Riverside, Riverside, CA 92521, USA.
*These authors contributed equally to this work.
†Corresponding author. Email: weihan@pku.edu.cn (W.H.); jrsun@iphy.ac.cn (J.R.S.); jing.shi@ucr.edu (J.S.)

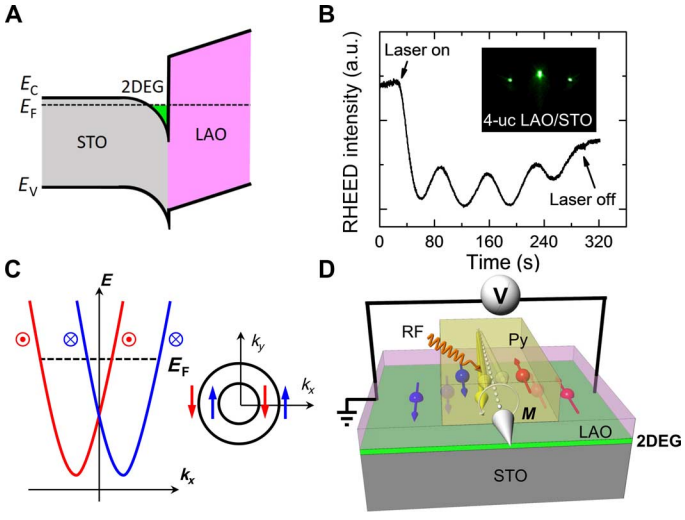

Fig. 1. The Rashba-split 2DEG between $SrTiO_3$ and $LaAlO_3$. (**A**) Schematic of 2DEG and the band alignment for the $SrTiO_3$ and $LaAlO_3$ heterostructures. (**B**) The RHEED oscillations of 4-UC $LaAlO_3$ growing on $SrTiO_3$. (**C**) The energy dispersion for a typical Rashba spin-split 2DEG. At the Fermi level, the outer and inner circles exhibit the opposite spin textures. (**D**) Schematic of the IEE measurements. The spin current is injected via spin pumping from Py under resonance condition. A voltage meter is used to probe the electric field generated because of the IEE of the Rashba-split 2DEG between two insulating oxides, $SrTiO_3$ and $LaAlO_3$.

where $\vec{M}$ is the magnetization vector, $\vec{H}_{\text{eff}}$ is the total effective magnetic field, γ is the gyromagnetic ratio, $M_S = |\vec{M}|$ is the saturation magnetization, and α is the Gilbert damping constant. At the resonance magnetic field (H_{res}) of ~470 Oe, the precessing magnetization of the Py electrode absorbs the microwave, and as a result, the measured amplitude of the complex transmission coefficient shows a minimum.

The black circles in Fig. 2B correspond to the measured voltage on the $SrTiO_3$/6-UC $LaAlO_3$ sample as a function of the magnetic field. It is clearly shown that the voltage signal is observed at the magnetic field around the resonance field of the Py on the $SrTiO_3$/6-UC $LaAlO_3$ sample (Fig. 2A), indicating that the measured voltage has a relationship with the spin pumping from Py under the resonance condition. We can analyze the measured voltage in terms of two major contributions (*4*, *16*): the IEE (V_{IEE}), due to the IEE of the spin polarization in the Rashba-split 2DEG, and the anomalous Hall effect of Py (V_{AHE}). The V_{IEE} and V_{AHE} are expected to show different symmetries around H_{res}, in which V_{IEE} shows a symmetric Lorentzian shape, whereas V_{AHE} exhibits an antisymmetric Lorentzian shape. A minor contribution is the Seebeck effect (V_{SE}), of which the sign does not depend on the Py magnetization direction (*16*). Thus, we can obtain all three of these contributions, V_{IEE}, V_{AHE}, and V_{SE}, on the basis of their different symmetries as a function of the magnetic field. First, the measured voltage is numerically simulated following the equation below

$$V(H) = V_S \frac{(\Delta H)^2}{(H - H_{\text{res}})^2 + (\Delta H)^2} + V_{\text{AHE}} \frac{-2\Delta H(H - H_{\text{res}})}{(H - H_{\text{res}})^2 + (\Delta H)^2} \quad (3)$$

where V_S is the voltage amplitude for the symmetric Lorentzian shape and ΔH is the half-linewidth. On the basis of the values for $V_S(+H)$ and

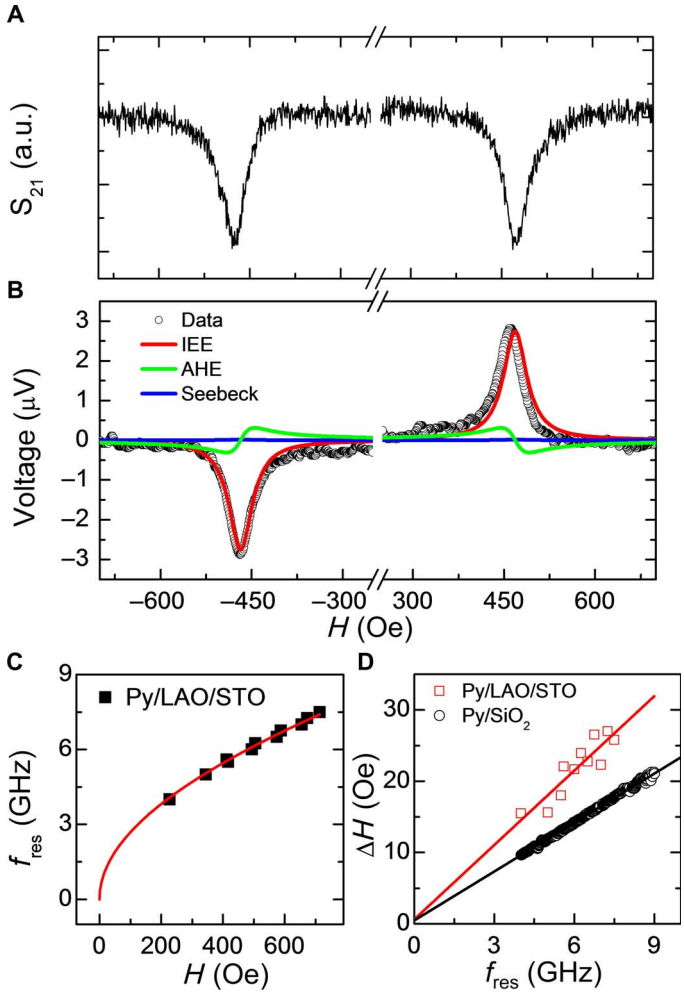

Fig. 2. The electrical detection of IEE of the Rashba-split 2DEG between $SrTiO_3$ and 6-UC $LaAlO_3$ at 300 K. (**A**) Representative FMR spectra of the Py electrode on the $SrTiO_3$/6-UC $LaAlO_3$ using a vector network analyzer with an RF frequency of 6 GHz. (**B**) The measured voltage (black circles) as a function of the magnetic field using a signal generator with a power of 1.25 W and an RF frequency of 6 GHz. The red, blue, and green lines are fitted curves that correspond to the voltages due to IEE of the injected spin current, the Seebeck effect, and the anomalous Hall effect of Py, respectively. (**C**) The resonance frequency (f_{res}) as a function of the resonance magnetic field (H_{res}). The solid line is a fitted curve based on the Kittel formula. (**D**) The half-linewidth (ΔH) versus the resonance frequency for Py on 6-UC $LaAlO_3$ (red squares) and SiO_2 (black circles) at 300 K, from which the Gilbert damping can be obtained from the slope of the linearly fitted curves.

$V_S(-H)$ obtained for the positive and negative H, we can determine the V_{IEE} based on $V_{\text{IEE}} = [V_S(+H) - V_S(-H)]/2$ and the V_{SE} based on $V_{\text{SE}} = [V_S(+H) + V_S(-H)]/2$. The red, blue, and green solid lines correspond to the numerically fitted components associated with IEE, the Seebeck effect, and the anomalous Hall effect, respectively. The resonance frequency (f_{res}) versus H_{res} is shown in Fig. 2C, and ΔH versus f_{res} for the 20-nm Py on the 6-UC $LaAlO_3$ is plotted in Fig. 2D. On the basis of these results, the demagnetization field of the 20-nm Py ($4\pi M_{\text{eff}}$) is 9.1×10^3 Oe using the Kittel formula

$$f_{\text{res}} = \left(\frac{\gamma}{2\pi}\right)[H_{\text{res}}(H_{\text{res}} + 4\pi M_{\text{eff}})]^{1/2} \quad (4)$$

The Gilbert damping constant of the 20-nm Py on the 6-UC $LaAlO_3$ is 0.0097, obtained from the slope of the linearly fitted curve (red line), which is significantly higher compared to that of the 20-nm Py (0.0064) grown on the SiO_2 substrate (black circles) (*35*). One major cause for the enhanced Gilbert damping parameter is the spin pumping into the Rashba-split 2DEG from the Py. On the basis of the enhanced Gilbert damping constants, we have estimated the spin mixing conductance ($G_{\uparrow\downarrow}$) between the magnetization of Py and the spins in the Rashba-split 2DEG to be 3.7×10^{19} m^2 and the injected spin current to be 6.7×10^6 A/m^2 using the model well established for spin pumping (*28*, *29*, *36*). The spin current value is in the range of previously reported values for the Rashba interface (*4*, *37*).

Next, the temperature dependence of IEE is studied. Figure 3A shows the representative voltages measured on the $SrTiO_3$/6-UC $LaAlO_3$ at various temperatures from 300 to 100 K. The V_{IEE} decreases quickly as the temperature decreases, and is no longer detectable below 200 K. The temperature dependence of the V_{IEE} on 2DEG between $SrTiO_3$ and 6-UC $LaAlO_3$ is summarized in Fig. 3B. As the temperature decreases, the 2DEG resistance shows a metallic behavior (Fig. 3C), measured by a two-probe method using the same Al wires for the IEE voltage measurements, which is consistent with previous studies (*19*, *20*). In addition, the junction resistance increases as the temperature decreases (Fig. 3C). The increase of the junction resistance might give rise to a lower value of the spin current across the $LaAlO_3$ layer and, consequently, a lower V_{IEE}.

To further study the temperature dependence behavior, we also measure two other samples: $SrTiO_3$/20-UC $LaAlO_3$ and $SrTiO_3$/40-UC $LaAlO_3$. The V_{IEE} quickly decreases as the temperature increases, as shown in Fig. 4 (A and B), which is very similar to that of $SrTiO_3$/6-UC $LaAlO_3$. In addition, R_J increases as temperature decreases, as shown in the inset of Fig. 4 (A and B). Figure 4C shows the normalized V^*_{IEE} by the RF microwave power ($V^*_{IEE} = V_{IEE}/P_{RF}$) as a function of the $LaAlO_3$ thickness. As the thickness increases, the V^*_{IEE} decreases.

The physical properties of the 2DEG between $SrTiO_3$ and $LaAlO_3$ could be largely modulated by a perpendicular electric field (*25*, *27*, *38*). To study the V_{IEE} as a function of the gate voltage at room temperature, we chose the heterostructures consisting of $SrTiO_3$ and 3-UC $LaAlO_3$ because of the large tunability of the electrical properties of the Rashba-split 2DEG at the interface. An electrode of silver paste is used on the other side of the $SrTiO_3$ substrate to serve as a back gate. The schematic of the measurement is illustrated in the inset of Fig. 5A, and Fig. 5A shows the spin voltage measured as a function of magnetic field with an RF power of 0.45 W under gate voltages of −20, −8, 0, 100, and 200 V. Clearly, no spin signal is observable under a gate voltage of −20 V, whereas clear spin signals are observed under a gate voltage (V_G) between 0 and 200 V. Figure 5B summarizes the spin voltage as a function of the back gate voltage measured at 300 K. We then checked the resistance of the 2DEG at the interface as a function of the gate voltage. It is noted that the resistance of the 2DEG greatly increases as the gate voltage becomes negative, as shown in Fig. 5C. The spin pumping, angular momentum transfer from Py to the spin polarization in the 2DEG, via such thick $LaAlO_3$ layer is very interesting. To the best of our understanding, the angular momentum could be transferred from the Py layer to spins in the 2DEG across this insulating $LaAlO_3$ layer via two possible mechanisms:

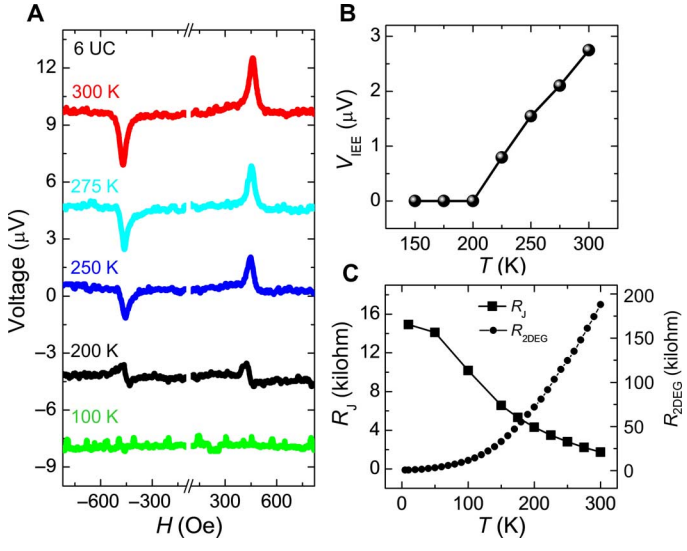

Fig. 3. The temperature dependence of IEE of the Rashba-split 2DEG between $SrTiO_3$ and 6-UC $LaAlO_3$. (**A**) The measured voltage on $SrTiO_3$/6-UC $LaAlO_3$ as a function of the magnetic field at 300, 275, 250, 200, and 100 K. (**B**) The temperature dependence of V_{IEE} for the Rashba-split 2DEG between $SrTiO_3$/6-UC $LaAlO_3$. (**C**) The temperature dependence of the junction resistance (R_J) between the Py and the 2DEG between $SrTiO_3$ and 6-UC $LaAlO_3$, and the 2DEG resistance (R_{2DEG}).

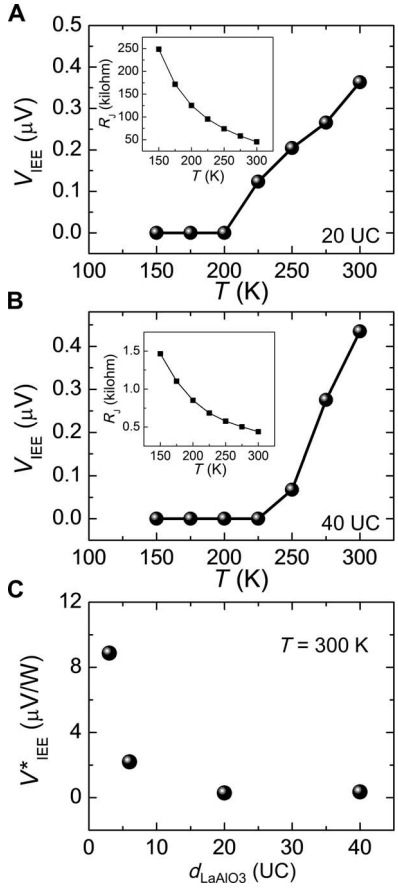

Fig. 4. The temperature and $LaAlO_3$ thickness dependences of IEE for the Rashba-split 2DEGs for $SrTiO_3/LaAlO_3$ with thickness up to 40 UC. (**A** and **B**) The temperature dependence of V_{IEE} of the Rashba-split 2DEGs for $SrTiO_3$/20-UC $LaAlO_3$ and $SrTiO_3$/40-UC $LaAlO_3$, respectively. Inset: Temperature dependence of R_J between the Py and the 2DEG between $SrTiO_3$ and $LaAlO_3$. (**C**) The normalized V^*_{IEE} as a function of the $LaAlO_3$ thickness.

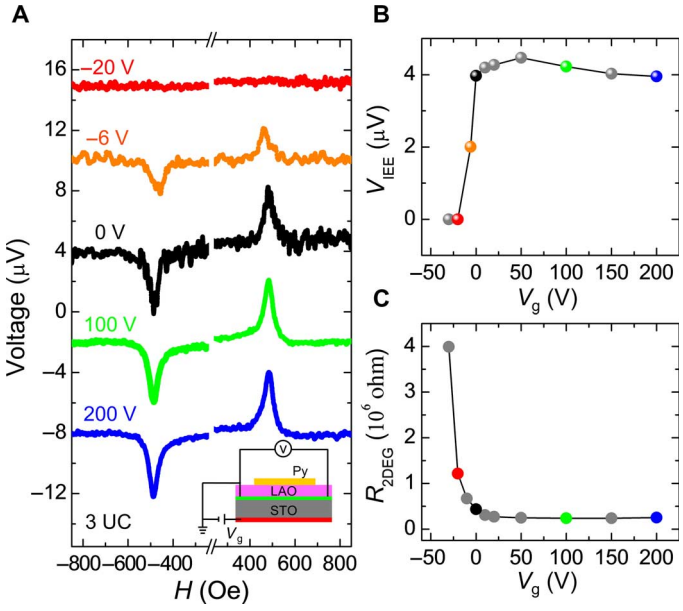

Fig. 5. The gate voltage dependence of IEE of the Rashba-split 2DEG between $SrTiO_3$ and 3-UC $LaAlO_3$. (**A**) The measured voltage on $SrTiO_3$/3-UC $LaAlO_3$ as a function of the magnetic field at 300 K for V_g = −20, −6, 0, 100, and 200 V. Inset: Schematic of the measurement under electric field using the $SrTiO_3$ as the dielectric layer. (**B**) The gate voltage dependence of V_{IEE} of the Rashba-split 2DEG between $SrTiO_3$ and 3-UC $LaAlO_3$. (**C**) The gate voltage dependence of 2DEG resistance between $SrTiO_3$ and 3-UC $LaAlO_3$.

spin tunneling across the $LaAlO_3$ layer and the angular momentum transfer via defects in the $LaAlO_3$ layer (for example, oxygen vacancies).

DISCUSSION

The temperature dependence of the V_{IEE} needs further theoretical and experimental studies. There are no existing mechanisms that could fully explain our observation, as discussed in the following. First, it is noted that there is no direct association of this behavior with the junction resistance, which affects the spin-pumping efficiency. As shown in Fig. 4 (A and B), although R_J varies over several orders of magnitude for various 2DEGs between $SrTiO_3$ and $LaAlO_3$ of 20 and 40 UC, the magnitudes of V_{IEE} for these two samples exhibit little difference, indicating that the IEE signal trend cannot simply be explained by the R_J variation. Especially, the disappearance of the V_{IEE} happens below a critical temperature of ~200 K in all three samples where R_J is very different. Second, we measure the temperature and thickness dependences of the mobility and carrier density of the interface, which are expected to affect the Rashba spin-orbit coupling and thus the spin-to-charge conversion efficiency. As shown in fig. S1, the temperature and thickness dependences of the mobility and carrier density show distinct trends compared to those of the V_{IEE}, indicating no obvious relationship between the carrier densities, the mobility at the interface, and the IEE signal. Third, we question whether there is strong magnetic impurity scattering at the interface, which could provide strong spin scattering to destroy the spin-momentum locking and make the V_{IEE} signal disappear. However, if the magnetic impurities exist, the spin scattering is expected to happen at all temperatures, especially at high temperatures. This is not likely the mechanism that could account for our results. Fourth, the exchange interactions between the Py and the interfacial 2DEG of $SrTiO_3$/$LaAlO_3$ might play an important role. If the spin injection and accumulation mechanisms are due to the exchange coupling between Py and 2DEG (*37*), the exchange interaction could be strongly temperature-dependent. However, exchange interaction is usually an energy scale that is determined by the overlap of wave functions and is temperature-independent. There is no cause for the exchange interactions to significantly disappear below ~200 K if temperature-dependent exchange interaction is the mechanism. Last, the observation might be related to the spin transport via the acoustic phonons in the $LaAlO_3$ layer, where the acoustic phonons could be chiral based on theoretical calculations for $LaAlO_3$ of fourfold square symmetry (*39*). However, there are yet no results indicating crystal structure symmetry change around the temperature of 200 K.

At room temperature, the gate voltage provides a powerful tool to tune the spin-to-charge conversion efficiency and even to turn the V_{IEE} signal on/off (Fig. 5 and fig. S2). The V_{IEE} (corresponding to the effective charge current), generated at negative gate voltages, is significantly lower, which indicates a lower effective spin-to-charge conversion, whereas the large spin signal and low resistance of the 2DEG under positive gate voltage indicate a larger spin-to-charge conversion. Because it is known that the dielectric constant of $SrTiO_3$ increases significantly at low temperatures (*40*), the gate voltage modulation of the V_{IEE} at low temperatures is expected to be significantly enhanced.

In summary, we have investigated the IEE in the Rashba-split 2DEG formed between two insulating oxides, $SrTiO_3$ and $LaAlO_3$, and demonstrated the gate voltage modulation of the V_{IEE} at room temperature. Our results reveal that the oxide interface can be used for efficient charge-to-spin conversion for the generation and detection of spin current beyond the applications for spin channels (*41*–*43*) and future electronics (*19*–*23*).

During the preparation of this manuscript, we became aware of the related spin pumping and IEE studies in $SrTiO_3$/2-UC $LaAlO_3$ at low temperature (T = 7 K) by Lesne *et al.* (*37*). Different from the said study, we report the strong modulation of IEE at room temperature by an electric field, the strong temperature dependence of the IEE, and the spin injection into the Rashba-split 2DEG across a series of $LaAlO_3$ thicknesses up to 40 UC.

MATERIALS AND METHODS

Material growth

The $LaAlO_3$ layers of 3 to 40 UC were grown on the top of (001)-oriented $SrTiO_3$ substrates (5 × 5 mm^2) via pulsed laser deposition with a laser fluence of 0.7 J cm^{-2} and a repetition rate of 1 Hz. During the growth, the $SrTiO_3$ substrates were held at a temperature of 800°C and in an oxygen pressure of 1 × 10^{-5} mbar. In situ RHEED oscillations were used to monitor the thickness of the $LaAlO_3$ layers. After deposition, the samples were in situ–annealed at 600°C for 1 hour and then cooled back to room temperature in 200 mbar of O_2. The details of the growth can be found in our earlier report (*44*).

Device fabrication

The device structure for the IEE measurement is illustrated in Fig. 1D. The 20-nm Py was deposited onto the $LaAlO_3$ via a shadow mask technique (size, ~3 × 4 mm^2) using RF magnetron sputtering, and a 3-nm Al was deposited in situ to prevent the oxidation of Py. The voltages were detected on the two ends of the 2DEG via Al bonding wires.

IEE measurement

The IEE response was measured using a digital lock-in amplifier (SRS Inc., SR830) by modulating the RF microwave power at a frequency

of 17 Hz for a better signal-to-noise ratio. The FMR measurement of Py magnetization dynamics was performed using a vector network analyzer (Agilent E5071C). For the IEE measurement, the RF microwave was set at a frequency of 6 GHz and an RF power of 1.25 W unless noted otherwise. Both FMR and IEE measurements were performed using the coplanar waveguide technique in the variable temperature insert of a Quantum Design Physical Properties Measurement System (PPMS).

SUPPLEMENTARY MATERIALS

Supplementary material for this article is available at http://advances.sciencemag.org/cgi/content/full/3/3/e1602312/DC1

fig. S1. The electron transport properties of the 2DEG.

fig. S2. The gate voltage dependence of IEE of the Rashba-split 2DEG between $SrTiO_3$ and 3-UC $LaAlO_3$.

REFERENCES AND NOTES

1. V. M. Edelstein, Spin polarization of conduction electrons induced by electric current in two-dimensional asymmetric electron systems. *Solid State Commun.* **73**, 233–235 (1990).
2. A. Manchon, H. C. Koo, J. Nitta, S. M. Frolov, R. A. Duine, New perspectives for Rashba spin–orbit coupling. *Nat. Mater.* **14**, 871–882 (2015).
3. K. Shen, G. Vignale, R. Raimondi, Microscopic theory of the inverse Edelstein effect. *Phys. Rev. Lett.* **112**, 096601 (2014).
4. J. C. R. Sánchez, L. Vila, G. Desfonds, S. Gambarelli, J. P. Attané, J. M. De Teresa, C. Magén, A. Fert, Spin-to-charge conversion using Rashba coupling at the interface between non-magnetic materials. *Nat. Commun.* **4**, 2944 (2013).
5. H. J. Zhang, S. Yamamoto, B. Gu, H. Li, M. Maekawa, Y. Fukaya, A. Kawasuso, Charge-to-spin conversion and spin diffusion in Bi/Ag bilayers observed by spin-polarized positron beam. *Phys. Rev. Lett.* **114**, 166602 (2015).
6. W. Zhang, M. B. Jungfleisch, W. Jiang, J. E. Pearson, A. Hoffmann, Spin pumping and inverse Rashba-Edelstein effect in NiFe/Ag/Bi and NiFe/Ag/Sb. *J. Appl. Phys.* **117**, 17C727 (2015).
7. M. Isasa, M. C. Martínez-Velarte, E. Villamor, C. Magén, L. Morellón, J. M. De Teresa, M. R. Ibarra, G. Vignale, E. V. Chulkov, E. E. Krasovskii, L. E. Hueso, F. Casanova, Origin of inverse Rashba-Edelstein effect detected at the Cu/Bi interface using lateral spin valves. *Phys. Rev. B* **93**, 014420 (2016).
8. J. B. S. Mendes, O. Alves Santos, L. M. Meireles, R. G. Lacerda, L. H. Vilela-Leão, F. L. A. Machado, R. L. Rodríguez-Suárez, A. Azevedo, S. M. Rezende, Spin-current to charge-current conversion and magnetoresistance in a hybrid structure of graphene and yttrium iron garnet. *Phys. Rev. Lett.* **115**, 226601 (2015).
9. W. Han, Perspectives for spintronics in 2D materials. *APL Mater.* **4**, 032401 (2016).
10. S. Dushenko, H. Ago, K. Kawahara, T. Tsuda, S. Kuwabata, T. Takenobu, T. Shinjo, Y. Ando, M. Shiraishi, Gate-tunable spin-charge conversion and the role of spin-orbit interaction in graphene. *Phys. Rev. Lett.* **116**, 166102 (2016).
11. W. Zhang, J. Sklenar, B. Hsu, W. Jiang, M. B. Jungfleisch, J. Xiao, F. Y. Fradin, Y. Liu, J. E. Pearson, J. B. Ketterson, Z. Yang, A. Hoffmann, Research Update: Spin transfer torques in permalloy on monolayer MoS_2. *APL Mater.* **4**, 032302 (2016).
12. D. MacNeill, G. M. Stiehl, M. H. D. Guimaraes, R. A. Buhrman, J. Park, D. C. Ralph, Control of spin–orbit torques through crystal symmetry in WTe_2/ferromagnet bilayers. *Nat. Phys.* 10.1038/nphys3933 (2016).
13. A. R. Mellnik, J. S. Lee, A. Richardella, J. L. Grab, P. J. Mintun, M. H. Fischer, A. Vaezi, A. Manchon, E.-A. Kim, N. Samarth, D. C. Ralph, Spin-transfer torque generated by a topological insulator. *Nature* **511**, 449–451 (2014).
14. C. H. Li, O. M. J. van't Erve, J. T. Robinson, Y. Liu, L. Li, B. T. Jonker, Electrical detection of charge-current-induced spin polarization due to spin-momentum locking in Bi_2Se_3. *Nat. Nanotechnol.* **9**, 218–224 (2014).
15. Y. Fan, P. Upadhyaya, X. Kou, M. Lang, S. Takei, Z. Wang, J. Tang, L. He, L.-T. Chang, M. Montazeri, G. Yu, W. Jiang, T. Nie, R. N. Schwartz, Y. Tserkovnyak, K. L. Wang, Magnetization switching through giant spin–orbit torque in a magnetically doped topological insulator heterostructure. *Nat. Mater.* **13**, 699–704 (2014).
16. Y. Shiomi, K. Nomura, Y. Kajiwara, K. Eto, M. Novak, K. Segawa, Y. Ando, E. Saitoh, Spin-electricity conversion induced by spin injection into topological insulators. *Phys. Rev. Lett.* **113**, 196601 (2014).
17. J.-C. Rojas-Sánchez, S. Oyarzún, Y. Fu, A. Marty, C. Vergnaud, S. Gambarelli, L. Vila, M. Jamet, Y. Ohtsubo, A. Taleb-Ibrahimi, P. Le Fèvre, F. Bertran, N. Reyren, J.-M. George, A. Fert, Spin to charge conversion at room temperature by spin pumping into a new type of topological insulator: α-Sn films. *Phys. Rev. Lett.* **116**, 096602 (2016).
18. Q. Song, J. Mi, D. Zhao, T. Su, W. Yuan, W. Xing, Y. Chen, T. Wang, T. Wu, X. H. Chen, X. C. Xie, C. Zhang, J. Shi, W. Han, Spin injection and inverse Edelstein effect in the surface states of topological Kondo insulator SmB_6. *Nat. Commun.* **7**, 13485 (2016).
19. H. Y. Hwang, Y. Iwasa, M. Kawasaki, B. Keimer, N. Nagaosa, Y. Tokura, Emergent phenomena at oxide interfaces. *Nat. Mater.* **11**, 103–113 (2012).
20. J. Mannhart, D. G. Schlom, Oxide interfaces—An opportunity for electronics. *Science* **327**, 1607–1611 (2010).
21. A. Ohtomo, H. Y. Hwang, A high-mobility electron gas at the $LaAlO_3/SrTiO_3$ heterointerface. *Nature* **427**, 423–426 (2004).
22. N. Reyren, S. Thiel, A. D. Caviglia, L. F. Kourkoutis, G. Hammerl, C. Richter, C. W. Schneider, T. Kopp, A.-S. Rüetschi, D. Jaccard, M. Gabay, D. A. Muller, J.-M. Triscone, J. Mannhart, Superconducting interfaces between insulating oxides. *Science* **317**, 1196–1199 (2007).
23. S. Stemmer, S. James Allen, Two-dimensional electron gases at complex oxide interfaces. *Annu. Rev. Mater. Res.* **44**, 151–171 (2014).
24. M. Basletic, J.-L. Maurice, C. Carrétéro, G. Herranz, O. Copie, M. Bibes, É. Jacquet, K. Bouzehouane, S. Fusil, A. Barthélémy, Mapping the spatial distribution of charge carriers in $LaAlO_3/SrTiO_3$ heterostructures. *Nat. Mater.* **7**, 621–625 (2008).
25. C. Cen, S. Thiel, G. Hammerl, C. W. Schneider, K. E. Andersen, C. S. Hellberg, J. Mannhart, J. Levy, Nanoscale control of an interfacial metal-insulator transition at room temperature. *Nat. Mater.* **7**, 298–302 (2008).
26. S. Hong, V. Diep, S. Datta, Y. P. Chen, Modeling potentiometric measurements in topological insulators including parallel channels. *Phys. Rev. B* **86**, 085131 (2012).
27. A. D. Caviglia, M. Gabay, S. Gariglio, N. Reyren, C. Cancellieri, J.-M. Triscone, Tunable Rashba spin-orbit interaction at oxide interfaces. *Phys. Rev. Lett.* **104**, 126803 (2010).
28. O. Mosendz, J. E. Pearson, F. Y. Fradin, G. E. W. Bauer, S. D. Bader, A. Hoffmann, Quantifying spin hall angles from spin pumping: Experiments and theory. *Phys. Rev. Lett.* **104**, 046601 (2010).
29. K. Ando, S. Takahashi, J. Ieda, Y. Kajiwara, H. Nakayama, T. Yoshino, K. Harii, Y. Fujikawa, M. Matsuo, S. Maekawa, E. Saitoh, Inverse spin-hall effect induced by spin pumping in metallic system. *J. Appl. Phys.* **109**, 103913 (2011).
30. K. Ando, S. Takahashi, J. Ieda, H. Kurebayashi, T. Trypiniotis, C. H. W. Barnes, S. Maekawa, E. Saitoh, Electrically tunable spin injector free from the impedance mismatch problem. *Nat. Mater.* **10**, 655–659 (2011).
31. F. D. Czeschka, L. Dreher, M. S. Brandt, M. Weiler, M. Althammer, I.-M. Imort, G. Reiss, A. Thomas, W. Schoch, W. Limmer, H. Huebl, R. Gross, S. T. B. Goennenwein, Scaling behavior of the spin pumping effect in ferromagnet-platinum bilayers. *Phys. Rev. Lett.* **107**, 046601 (2011).
32. K. Ando, E. Saitoh, Observation of the inverse spin Hall effect in silicon. *Nat. Commun.* **3**, 629 (2012).
33. L. Landau, E. Lifshitz, On the theory of the dispersion of magnetic permeability in ferromagnetic bodies. *Phys. Z. Sowjet.* **8**, 153 (1935).
34. T. L. Gilbert, A phenomenological theory of damping in ferromagnetic materials. *IEEE Trans. Magn.* **40**, 3443–3449 (2004).
35. Y. Zhao, Q. Song, S.-H. Yang, T. Su, W. Yuan, S. S. P. Parkin, J. Shi, W. Han, Experimental investigation of temperature-dependent Gilbert damping in permalloy thin films. *Sci. Rep.* **6**, 22890 (2016).
36. Y. Tserkovnyak, A. Brataas, G. E. W. Bauer, B. I. Halperin, Nonlocal magnetization dynamics in ferromagnetic heterostructures. *Rev. Mod. Phys.* **77**, 1375–1421 (2005).
37. E. Lesne, Y. Fu, S. Oyarzun, J. C. Rojas-Sánchez, D. C. Vaz, H. Naganuma, G. Sicoli, J.-P. Attané, M. Jamet, E. Jacquet, J.-M. George, A. Barthélémy, H. Jaffrés, A. Fert, M. Bibes, L. Vila, Highly efficient and tunable spin-to-charge conversion through Rashba coupling at oxide interfaces. *Nat. Mater.* **15**, 1261–1266 (2016).
38. S. Thiel, G. Hammerl, A. Schmehl, C. W. Schneider, J. Mannhart, Tunable quasi-two-dimensional electron gases in oxide heterostructures. *Science* **313**, 1942–1945 (2006).
39. L. Zhang, Q. Niu, Chiral phonons at high-symmetry points in monolayer hexagonal lattices. *Phys. Rev. Lett.* **115**, 115502 (2015).
40. K. A. Müller, H. Burkard, $SrTiO_3$: An intrinsic quantum paraelectric below 4 K. *Phys. Rev. B* **19**, 3593–3602 (1979).
41. N. Reyren, M. Bibes, E. Lesne, J.-M. George, C. Deranlot, S. Collin, A. Barthélémy, H. Jaffrès, Gate-controlled spin injection at $LaAlO_3/SrTiO_3$ interfaces. *Phys. Rev. Lett.* **108**, 186802 (2012).
42. W. Han, X. Jiang, A. Kajdos, S.-H. Yang, S. Stemmer, S. S. P. Parkin, Spin injection and detection in lanthanum- and niobium-doped $SrTiO_3$ using the Hanle technique. *Nat. Commun.* **4**, 2134 (2013).
43. R. Ohshima, Y. Ando, K. Matsuzaki, T. Susaki, M. Weiler, S. Klingler, H. Huebl, E. Shikoh, T. Shinjo, S. T. B. Goennenwein, M. Shiraishi, Realization of *d*-electron spin transport at room temperature at a $LaAlO_3/SrTiO_3$ interface. arXiv:1601.07568v1 (2016).
44. Y. Lei, Y. Li, Y. Z. Chen, Y. W. Xie, Y. S. Chen, S. H. Wang, J. Wang, B. G. Shen, N. Pryds, H. Y. Hwang, J. R. Sun, Visible-light-enhanced gating effect at the $LaAlO_3/SrTiO_3$ interface. *Nat. Commun.* **5**, 5554 (2014).

Acknowledgments: We thank Q. Niu, X. C. Xie, and L. Zhang for the fruitful discussion. **Funding:** We acknowledge financial support from the National Basic Research Programs of China (973 Program grant nos. 2015CB921104, 2016YFA0300701, 2014CB920902, and 2013CB921901) and the National Natural Science Foundation of China (NSFC grant nos. 11574006 and 11520101002). **Author contributions:** J. Shi, J. Sun, and W.H. proposed and supervised the study. Q.S. performed the device fabrication and IEE measurements. Q.S. and H.Z. analyzed the data. H.Z. and J. Sun grew the $SrTiO_3/LaAlO_3$ samples and performed the characterization of the electrical properties of the 2DEG. Q.S., J. Shi, J. Sun, and W.H. wrote the manuscript. All authors commented on the manuscript and contributed to its final version. **Competing interests:** The authors declare that they have no competing interests. **Data and materials availability:** All data needed to evaluate the conclusions in the paper are present in the paper and/or the Supplementary Materials. Additional data related to this paper may be requested from the authors.

Submitted 21 September 2016
Accepted 3 February 2017
Published 17 March 2017
10.1126/sciadv.1602312

Citation: Q. Song, H. Zhang, T. Su, W. Yuan, Y. Chen, W. Xing, J. Shi, J. Sun, W. Han, Observation of inverse Edelstein effect in Rashba-split 2DEG between $SrTiO_3$ and $LaAlO_3$ at room temperature. *Sci. Adv.* **3**, e1602312 (2017).

ScienceAdvances
AAAS

Observation of inverse Edelstein effect in Rashba-split 2DEG between $SrTiO_3$ and $LaAlO_3$ at room temperature

Qi Song, Hongrui Zhang, Tang Su, Wei Yuan, Yangyang Chen, Wenyu Xing, Jing Shi, Jirong Sun and Wei Han (March 17, 2017)
Sci Adv 2017, 3:.
doi: 10.1126/sciadv.1602312